Desalination and Water Treatment
www.deswater.com
doi: 10.5004/dwt.2023.30215

316 (2023) 431–444
December

Removal of chemical oxygen demand from slaughterhouse wastewater by electrocoagulation in continuous mode: isothermal, kinetic and adsorption study

Santiago A. Tuesta-Tinoco[a,b], Paola L. Alcántara-Romero[a], Ricardo A. Yuli-Posadas[c], María E. King-Santos[a,d], Walter F. Zaldivar-Alvarez[a], Adolfo La Rosa-Toro[e], Warren Reátegui-Romero[a,*]

[a]*Facultad de Ingeniería Química y Textil (FIQT), Universidad Nacional de Ingeniería (UNI), Av. Túpac Amaru 210, Rímac, Lima 15333, Peru, emails: wreategui@uni.edu.pe (W. Reátegui-Romero), stuesta.uni@gmail.com (S.A. Tuesta-Tinoco), alcantara_romero@hotmail.com (P.L. Alcántara-Romero), mkings@uni.edu.pe (M.E. King-Santos), wzaldivar@uni.edu.pe (W.F. Zaldivar-Alvarez)*
[b]*Esmeralda Corp. S.A.C., Carretera Panamericana Sur km 18.5 mz. G lt. 1, Chorrillos, Lima 15058, Peru*
[c]*Universidad Nacional de San Marcos, Calle German Amezaga N° 375, Edificio Jorge Basadre, Ciudad Universitaria, Lima 1, Peru, email: ryulip@unmsm.edu.pe*
[d]*Facultad de Ingeniería Ambiental (FIA), Universidad Nacional de Ingeniería (UNI), Av. Tupac Amaru 210, Rimac, Lima 15333, Peru*
[e]*Laboratorio de Electroquímica Aplicada, Universidad Nacional de Ingeniería (UNI), Av. Túpac Amaru 210, Rimac, Lima 15333, Peru, email: toro@uni.edu.pe*

Received 1 August 2023; Accepted 8 December 2023

ABSTRACT

The objective of this work was to study the effect of hydraulic retention time on the removal efficiency of the chemical oxygen demand (COD), and to evaluate the energy consumption (EC) using the electrocoagulation process in continuous mode with aluminum and iron electrodes. Three volumetric flows of 10, 15 and 22.5 L/h, with hydraulic retention times of 0.5, 0.33 and 0.22 h were studied. The COD and turbidity ranges were 5,400–9,500 mg/L and 2,000–2,600 NTU, respectively. Experimental data were analyzed using kinetic equations: pseudo-first-order and pseudo-second-order models considering both isothermal and non-isothermal conditions. Under optimal conditions, voltage 8 V and hydraulic retention time of 0.33 h, the COD and turbidity removal efficiencies were 62.2% and 99.5%, and 51.2% and 94.5% with aluminum and iron electrodes in a time 60 min, respectively. The results showed that the data fit the pseudo-second-order isotherm model (R^2 = 0.997–1.000). The study showed that the EC process strongly depends on hydraulic retention time.

Keywords: Al/Fe electrodes; Oil and grease, Turbidity; Pseudo-first-order model; Pseudo-second-order model

1. Introduction

Environmental pollution in the world has increased notably in recent decades. With a growing world population, there is a greater demand for water both for human consumption as well as for industrial uses. The meat industry generates large amounts of contaminated water, and we have worked with this wastewater. Slaughterhouse wastewater exhibits a high organic [1–3] and inorganic load; high suspended solids content, etc. [2,4]. The main sources

* Corresponding author.

of organic materials in the slaughterhouse wastewater are blood, fat oil and grease, etc. [1,2,5]. The wastewater has a high strength in terms of biochemical oxygen demand, chemical oxygen demand (COD), suspended solids, nitrogen, and phosphorus [6], compared to domestic wastewaters [2,7]. When wastewater from the red meat processing industry is discharged without treatment into the sewage system, it leads to dissolved oxygen depletion, odor release, sludge deposits, and floating scum [4,8]. There are several methods to remove contaminants from water, such as chemical coagulation and flocculation, by adding chemicals [9,10]; electrocoagulation (EC)/electroflotation applying electrical energy [11]; biological processes with the use of microorganisms [12]; filtration, resin exchange, advanced oxidation (Fenton/electro-Fenton) [13,14]; etc. The electrocoagulation process is a method that generates coagulants from the forced oxidation reaction at the anode or positive pole, and reduction reactions occur at the cathode or negative pole. This is possible due to the current flow that circulates between the poles. The electrocoagulation does not require external chemicals and removes any size of suspended solids, oil, and grease, as well as heavy metals [15]. The sacrificial electrodes used in this process are made of iron and aluminum. The mechanism of forming the coagulant with Fe electrode is explained [16–21]:

Oxidation reaction at the anode: Fe

Alkaline conditions (pH < 8.7):

$$\mathrm{Fe(s)} \rightarrow \mathrm{Fe^{2+}(aq)} + 2\mathrm{e^-} \quad (1)$$

The ferrous-ion forms ferrous hydroxide [Eq. (2)].

$$\mathrm{Fe^{2+}(aq)} + 2\mathrm{OH^-(aq)} \rightarrow \mathrm{Fe(OH)_2(s)} \quad (2)$$

Under these conditions the ferrous-ion forms ferric hydroxide [Eq. (3)].

$$4\mathrm{Fe^{2+}(aq)} + \mathrm{O_2(g)} + 10\mathrm{H_2O(l)} \rightarrow 4\mathrm{Fe(OH)_3(s)} + 8\mathrm{H^+(aq)} \quad (3)$$

Water electrolysis [Eq. (4)].

$$2\mathrm{H_2O(aq)} - 4\mathrm{e^-} \rightarrow \mathrm{O_2(g)} + 4\mathrm{H^+(aq)} \quad (4)$$

Reduction reaction at the cathode [Eq. (5)].

$$6\mathrm{H_2O(aq)} + 6\mathrm{e^-} \rightarrow 3\mathrm{H_2(g)} + 6\mathrm{OH^-(aq)} \quad (5)$$

Ferric-ions electrochemically generated may form monomeric ions, ferric hydroxo complex with OH^-(aq)- ions, and polymeric species, which finally transform into $Fe(OH)_3$(s) [22]: $Fe(OH)^{2+}$(aq), $Fe(OH)_2^+$(aq), $Fe(H_2O)_4(OH)^{2+}$(aq), $Fe(H_2O)_5(OH)^{2+}$(aq), $Fe_2(H_2O)_6(OH)_4^{2+}$(aq), $Fe(H_2O)_6^{3+}$(aq), $Fe_2(H_2O)_8(OH)_2^{4+}$(aq). These species are influenced by pH (4–9), and have strong affinity for counterions, which causes the coagulation and removal of contaminants from the water. When the pH of the medium is higher than 9, the dominant species is $Fe(OH)_4^-$(aq), which does not contribute to coagulation. The mechanism of coagulant formation using the Al electrode is explained [16,23–26]:

Oxidation reaction at the anode: Al

$$\mathrm{2Al(s)} \rightarrow \mathrm{2Al^{3+}(aq)} + 6\mathrm{e^-} \quad (6)$$

Reduction reaction at the cathode, [Eq. (5)]:

In solution, the generated Al^{3+}(aq) and OH^-(aq)-ions react to form $Al(OH)_3$(s) [Eq. (7)].

$$\mathrm{2Al^{3+}(aq)} + 6\mathrm{H_2O(l)} \rightarrow \mathrm{2Al(OH)_3(s)} + 3\mathrm{H_2(g)} \quad (7)$$

The cathode may also be chemically attacked [Eq. (8)] by OH^-(aq)-ions generated during H_2(g) evolution at high pH [27].

$$\mathrm{2Al(s)} + 6\mathrm{H_2O(l)} + 2\mathrm{OH^-(aq)} \rightarrow \mathrm{2Al(OH)_4^-(aq)} + 3\mathrm{H_2(g)} \quad (8)$$

This complex anion is soluble and appears at pH > 10, causing the sludge redissolution [28]. Thus, it does not help to remove contaminants from wastewater. The EC process with aluminum electrodes should be done at pH < 10 [26]. In 4–9 pH range, several monomeric and polymeric species are formed [26,29,30]: $Al(OH)^{2+}$(aq), $Al(OH)_2^+$(aq), $Al_2(OH)_2^{4+}$(aq), $Al(OH)_3$(s), $Al_6(OH)_{15}^{3+}$(aq), $Al_7(OH)_{17}^{4+}$(aq), $Al_8(OH)_{20}^{4+}$(aq), $Al_3(OH)_4^{5+}$(aq), $Al_{13}(OH)_{34}^{5+}$(aq), $Al_{13}(OH)_{32}^{7+}$(aq), and $Al_{13}O_4(OH)_{24}^{7+}$(aq). The surface of these compounds has large amounts of positive charge, which can lead to adsorption electrochemistry neutralization and net catching reaction [26,31]. The flocculation process at pH lower than 6.5 is explained as precipitation, while for higher values are explained as adsorption [30,31]. The passage of electric current dissolves the anodes and its consumption per unit volume of treated effluent is expressed by [Eq. (9)]. energy consumption per unit volume of treated effluent can be calculated by [Eq. (10)] or per unit organic load removed (COD) [Eq. (11)], respectively [32] and [Eq. (10)] [33]:

$$\mathrm{ELC}\left(\frac{\mathrm{kg}}{\mathrm{m^3}}\right) = \frac{M \cdot I_m \cdot t}{n \cdot F \cdot V_t} \quad (9)$$

$$\mathrm{SEC_{VOL}}\left(\frac{\mathrm{kWh}}{\mathrm{m^3}}\right) = \frac{0.001}{3600} \times \frac{U \cdot I_m \cdot t}{V_t} \quad (10)$$

$$\mathrm{SEC_{COD}}\left(\frac{\mathrm{kWh}}{\mathrm{kgCOD}}\right) = \frac{1}{3600} \times \frac{U \cdot I_m \cdot t}{V_t\left(\mathrm{COD_0} - \mathrm{COD_t}\right)} \quad (11)$$

where M is the molar mass (g/mol) of the electrode; F is the Faraday's constant (96,500 C/mol); U (voltage, V); I_m (mean current intensity, A); t (EC operating time, s); V_t (treated volume, m^3); and COD_0 and COD_t (initial and at time t COD concentrations, mg/L). The objective of this research work was to study the effect of hydraulic retention time on the removal efficiency of chemical oxygen demand, and evaluate energy consumption using Al and Fe electrodes, as primary treatment of wastewater from a slaughterhouse.

2. Materials and methods

2.1. Sample collection

The wastewater was initially pre-treated by screening and sedimentation and sent to a 170 m^3 tank (Fig. 1).

Fig. 1. Storage of meat wastewater in the equalizing tank after pre-treatment.

Table 1 shows the physical–chemical characteristics of the effluent to be treated corresponding to the mean values of six samples taken in a 3-month period.

Table 1
Physical–chemical characterization of the meat effluent in the equalizing tank

Parameter	Unit	Range
pH		7.0–7.8
Chemical oxygen demand	mg/L	5,400–9,500
Biochemical oxygen demand	mg/L	2,300–3,950
Turbidity	NTU	2,000–2,600
Total suspended solids	mg/L	800–1,800
Total Kjeldahl nitrogen	mg/L	170–300
Total phosphorus	mg/L	25–55
Oil & grease	mg/L	80–86
Thermotolerant coliforms	MPN (100 mL)	1.6–2.4.109

2.2. Experimental set-up

Fig. 2 shows the scheme for wastewater treatment in continuous flow by EC. The reactor was designed to treat 5 L of wastewater, with internal dimensions of 0.13 m × 0.20 m × 0.25 m of transparent plexiglass material, with a thickness of 0.009 m. The dimensions of the electrodes (3 anodes and 2 cathodes) were 0.15 m × 0.133 m × 0.0016 m. They were separated by 0.03 m. The experiments were performed with the electrodes installed in vertical position and in monopolar connection. Wastewater feed treated wastewater discharge and sludge discharge were controlled

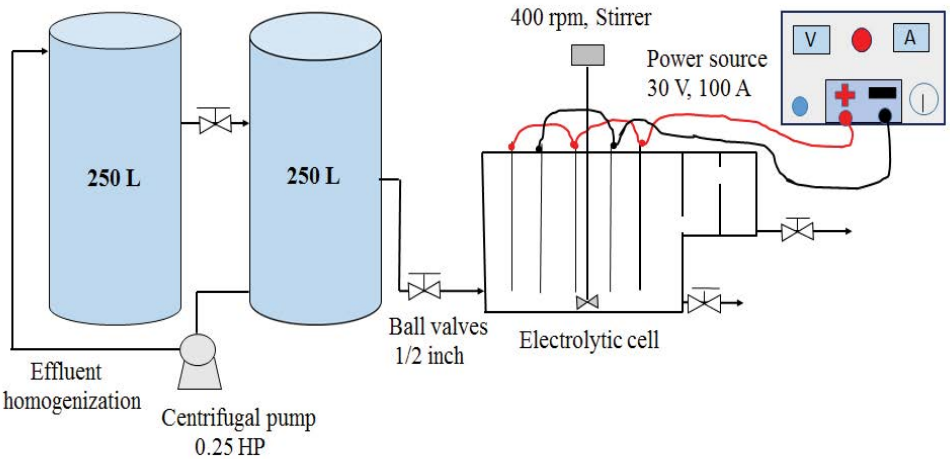

Fig. 2. Continuous flow electrocoagulation system: electrolytic cell, power source and homogenizer tank.

with 1/2 inch ball valves. Two tanks of 250 L were used to homogenize the effluent, and a 0.25 HP centrifugal pump was required to recirculate the effluent. To prevent sludge from entering the reactor, the feed pipe was installed at half the height of the tank, and the recirculation at 0.20 m from the base of the tank. The characteristics of the power source were a voltage variation range of 0–30 V and an amperage of 0–100 A. The samples for analysis of the different parameters were collected at 0, 10, 25, 45 and 60 min. The electrodes were weighed after each time indicated. The experiments were carried out with three volumetric flows of 10, 15 and 22.5 L/h, which correspond to hydraulic retention times of 0.5, 0.33 and 0.22 h, respectively. The COD and turbidity ranges were 5,400 to 9,500 mg/L and 2,000 to 2,600 NTU, respectively. In all the tests carried out, the applied voltage was 8 V. This value was selected in a previous research work in discontinuous mode with the same effluent [33]. Experimental data were analyzed using kinetic equations of pseudo-first-order and pseudo-second-order models considering both isothermal and non-isothermal, and also considering the linearization and non-linearization of the respective models of removal of the organic load for both configurations of the materials aluminum and iron were used for anodes and cathodes. To determine the mass of the electrodes, a Henkel precision electronic balance with 5 mg readability was equipped. Temperatures were measured using a multi-thermometer-91000-050/F. A pH meter EC-HI98129 Hanna Instruments was used to measure pH. A 2100AN Turbidimeter Hach model was used to measure turbidity. A HI 83980 COD Reactor-Hanna Instruments Thermoreactor and a HI 83224 WTP-Hanna Instruments multiparameter photometer were used to measure COD. Hanna Instruments and Hach are headquartered in Woonsocket, Rhode Island and Loveland, Colorado in United States of America, respectively.

2.3. Equilibrium studies

The amount of organic load coagulated at equilibrium, q_e (mg/g), was calculated using Eq. (12) [34,35].

$$q_e = \left(\frac{C_0 - C_e}{W}\right) \cdot V_t \tag{12}$$

where C_0 (mg/L) and C_e (mg/L) are the initial and at equilibrium COD concentration in the liquid phase. V_t is the treated volume (L) and W (g) is the mass of the coagulant estimated from the Faraday's Law according to Eq. (13) [34].

$$W = \frac{M \cdot I \cdot t}{nF} \tag{13}$$

where M is the molar mass (g/mol) of the electrode (anode) (M_{Fe} = 55.85 and M_{Al} = 26.98); I is the current (A); t is the electrocoagulation time in seconds; n is the number of electrons; F is the Faraday's constant (96,500 C/mol). The removal efficiency was calculated using Eq. (14):

$$\%\ \text{removal efficiency} = \left(\frac{C_0 - C_t}{C_0}\right) \times 100\% \tag{14}$$

2.4. Isothermal models of electrocoagulation–flotation kinetics

To predict the concentration of organic load expected for a non-stationary state over a certain operating time, both volumetric flow and voltage were determining parameters in the kinetic control of the continuous EC experiments. The experimental concentrations were modeled in the form of linear and non-linear regression, using the Microsoft Excel 2019 Solver tool.

2.4.1. Pseudo-first-order and pseudo-second-order kinetic model

A kinetic model is a mathematical representation of the rate at which physical–chemical processes take place. Adsorption kinetics controls the rate of adsorption. It also determines the time required to reach equilibrium of the adsorption process. Kinetic models provide information about the adsorption pathways and the likely mechanism involved [36]. The speed of these adsorption processes varies from very fast to very slow [37,38]. However, the process is controlled by the slowest stage [36]. The control mechanism of the organic load sorption process was analyzed with pseudo-first-order kinetic models in its non-linear form [Eq. (15)] [39,40]; linear form [Eq. (16)] [39,41–44]; pseudo-second-order in its non-linear form [Eq. (17)] [40]; and linear forms type I [Eq. (18)] and type II [Eq. (19)] [43,45–48]. Lagergren's first-order rate equation is widely used to describe the adsorption kinetics of different pollutants from liquid phase into the porous media [46].

$$q_t = q_e \cdot \left(1 - e^{-k_1 t}\right) \tag{15}$$

$$\ln\left(q_e - q_t\right) = \ln q_e - k_1 t \tag{16}$$

where q_e and q_t (mg/g) are the adsorption capacities at equilibrium and at time t, respectively. k_1 (min^{-1}) is the rate constant of pseudo-first-order adsorption. The straight-line plot of $\ln(q_e - q_t)$ against t gives k_1 as slope and intercept equal to $\ln(q_e)$. Hence, the amount of adsorbed solute per gram of sorbent at equilibrium (q_e) and the first-order sorption rate constant (k_1) can be evaluated from the slope and the intercept [41].

$$q_t = \frac{k_2 q_e^2 t}{1 + k_2 q_e t} \tag{17}$$

$$\frac{t}{q_t} = \frac{1}{k_2 q_e^2} + \frac{t}{q_e} \tag{18}$$

$$\frac{1}{q_e} = \frac{1}{q_e - q_t} - \left(k_2\right) t \tag{19}$$

where k_2 (g/mg·min) is the rate constant of the pseudo-second-order equation. A plot of (t/q_t) vs. (t) was used to calculate k_2 and q_e (mg/g) which is the adsorption capacity at equilibrium, and q_t (mg/g) is the amount adsorbed at time t (min). The initial adsorption rate h (mg/g·min) was evaluated with Eq. (20).

$$h = k_2 q_e^2 \tag{20}$$

2.5. Non-isothermal kinetics model of pseudo-first-order and pseudo-second-order adsorption of electroflotation–electrocoagulation

To understand the effect of temperature on adsorption process, thermodynamic parameters should be determined at various temperatures [49]. The energy of activation for adsorption of the organic load can be determined by both the pseudo-first-order constant (k_1) and pseudo-second-order rate constants (k_2) expressed in Arrhenius form [Eq. (21)] [50].

$$k_n = k_0 \cdot e^{-\frac{E_a}{RT}} \tag{21}$$

where k_0 is the constant of the equation (g/mg·min); E_a is the energy of activation (J/mol); R is the gas constant (8.314 J/mol·K); and T is the temperature (K). If we replace Eq. (21) in the mathematical expression (pseudo-first-order kinetics model), it gives rise to Eq. (16), and, we obtain Eq. (22) for:

$$\ln q_e - \ln\left(q_e - q_t\right) = \int_0^t k_0 \cdot e^{-\frac{E_a}{RT}} dt \tag{22}$$

While, similarly, for the mathematical expression (pseudo-second-order kinetics model) which gives rise to Eq. (13) by replacing Eq. (21), we obtain Eq. (23) for:

$$\frac{1}{q_e - q_t} - \frac{1}{q_e} = \int_0^t k_0 \cdot e^{-\frac{E_a}{RT}} dt \tag{23}$$

Experimentally, it is observed that the temperature variation with time has a good linear behavior (Fig. 6). Therefore, it is possible to assume ($T = T_0 + \beta t$ so that $dT/dt = \beta$). Replacing this assumption into Eq. (2), and operating properly, Eq. (24) can be obtained. At the same way, by replacing the linear temperature gradient assumption into Eq. (23), Eq. (25) can be obtained. Both Eq. (24) and Eq. (25) must be solved by iteration to determine q_t. This mathematical training can be reviewed by Lyon [51].

$$\ln\left[\ln\left(q_e\right) - \ln\left(q_e - q_t\right) + \frac{k_o R T_o^2}{\beta E_a} e^{-\frac{E_a}{RT_o}}\right] - 2\ln\left(T\right) = \ln\left(\frac{k_o R}{\beta E_a}\right) - \frac{E_a}{RT} \tag{24}$$

$$\ln\left(\frac{1}{q_e - q_t} - \frac{1}{q_e} + \frac{k_o R T_o^2}{\beta E_a} e^{-\frac{E_a}{RT_o}}\right) - 2\ln\left(T\right) = \ln\left(\frac{k_o R}{\beta E_a}\right) - \frac{E_a}{RT} \tag{25}$$

2.6. Adsorption kinetics in a continuous process before reaching the steady state

The steady state mass balance is represented by Eq. (26). The experiments were carried out in an open stirred reactor. Thus, there is an equality between the concentrations of the chemical oxygen demand inside the reactor ($[COD]_{in}$) and at the reactor outlet ($[COD]_{out}$). The volumetric flow rates at the reactor inlet and outlet are equal ($Q = Q_{in} = Q_{out}$).

$$Q_{in} C_{COD,in} - Q_{out} C_{COD,out} + V \frac{d\left[COD\right]}{dt} = 0 \tag{26}$$

During the continuous EC process, COD concentrations followed a decreasing exponential profile, hence considering stationary states were not reached. Then the proposed mathematical modeling [Eq. (27)] [32] is adjusted to the experimental data.

$$C_t = A_1 e^{-B_1 t} + C_\infty \tag{27}$$

where A_1 and B_1 are constants. C_t (mg/L) and C_∞ (mg/L) are the COD concentrations at time t and at equilibrium, respectively. The capacity of adsorption at time t, q_t (mg/g), for a EC continuous system was calculated using [Eq. (28)] based on Eq. (12):

$$q_t = \left(\frac{C_o - C_t}{W}\right) Q \tag{28}$$

where Q (L/h) is the flow rate and W (g/h) is the specific electrode consumption assuming a Faraday's Law linear dissolution of the anodes. C_0 is the initial COD concentration according to [Eq. (28)] $C_0 = A_1 + C_{(\infty)}$. Consequently, by operating properly, q_t can be obtained in terms of A_1, B_1 and the EC continuous parameters, expressed in Eq. (29).

$$q_t = \frac{A_1 \cdot Q\left(1 - e^{-B_1 t}\right)}{W} \tag{29}$$

Compared to the pseudo-first-order q_t non-linear form in Eq. (15), we can obtain experimental values for q_e and k_1 [Eq. (30)].

$$q_e = \frac{A_1 \cdot Q}{W} \tag{30}$$

Based on the work done by Tounsi et al. [32], we similarly propose a decreasing fractional profile for modeling COD concentrations [Eq. (31)].

$$C_t = C_o + \frac{A_2 \cdot t}{1 + B_2 \cdot t} \tag{31}$$

where A_2 and B_2 are constants. C_o is the initial COD concentration according to Eq. (32). By operating properly, q_t can be obtained in terms of A_2, B_2 and the EC continuous parameters, expressed in Eq. (32). The capacity of adsorption at time t, q_t (mg/g) for a EC continuous system was calculated using Eq. (28).

$$q_t = -\frac{A_2 \cdot Q \cdot t}{W\left(1 + B_2 \cdot t\right)} \tag{32}$$

By comparing Eq. (32) with the pseudo-second-order non-linear form Eq. (17), values for q_e and k_2 [Eq. (33)] can be obtained experimentally.

$$q_e = \frac{A_2 \cdot Q}{W \cdot B_2} \qquad q_e k_2 = B_2 \tag{33}$$

3. Results and discussion

3.1. Influence of hydraulic retention time on energy consumption

Tables 2 and 3 show in each interval time the mean current intensity and the energy consumption (SEC) per cubic meter of treated water (kWh/m^3) at different hydraulic retention time using Al and Fe electrodes. There is a remarkable trend between hydraulic retention time (HRT) and applied current intensity as well as SEC, for all cases. The lower flow rate or volumetric flow generates the higher HRT value, thus requiring higher electrical current and power consumption. At 8 V, the energy consumed per cubic meter for continuous EC has almost the same value for any time. For instance, at HRT: 0.33 h (15 L/h), for Al and Fe electrodes the SEC_{VOL} were 4.71 and 4.66 kWh/m^3. The specific energy consumption per unit of treated volume is slightly higher Al electrodes at any time. However, as Table 4 presents, the energy consumption per kg of COD removed using Al electrodes were 1.27 ± 0.07, 0.92 ± 0.05 and 0.65 ± 0.09 kWh/kg COD while using Fe electrodes the SEC_{COD} were 1.50 ± 0.17, 1.16 ± 0.23 and 0.85 ± 0.20 kWh/kg COD. The electrocoagulation process with Al electrodes has lower specific energy consumption per unit of COD removed regarding Fe electrodes at an average of 0.22 kWh/kg COD for any hydraulic retention time. In addition, it is notorious that the rate of decrease in SEC_{COD} is always lower with Al electrodes, which favors the EC process in shorter operation times with respect to Fe electrodes. Therefore, it is convenient to work at longer operating times with Fe electrodes to reduce the energy consumption per COD removed. In other research, with cattle slaughterhouse effluent using Al electrodes with a flow rate of 1.62 L/h, the energy consumption was 0.87 kWh/m^3 with a hydraulic retention time of 60 min [52].

Table 2
Energy consumption per m^3 of treated water at voltage 8 V with Al electrodes

HRT (h)		0.50		0.33		0.22
Interval (min)	Mean intensity (A)	Energy consumption (kWh/m^3)	Mean intensity (A)	Energy consumption (kWh/m^3)	Mean intensity (A)	Energy consumption (kWh/m^3)
0–10	9.25	7.40	8.68	4.63	8.84	3.14
0–25	9.28	7.42	8.88	4.74	8.92	3.17
0–45	9.23	7.38	8.88	4.74	8.94	3.18
0–60	9.23	7.38	8.88	4.74	8.94	3.18

Table 3
Energy consumption per m^3 of treated water at voltage 8 V with Fe electrodes

HRT (h)		0.50		0.33		0.22
Interval (min)	Mean intensity (A)	Energy consumption (kWh/m^3)	Mean intensity (A)	Energy consumption (kWh/m^3)	Mean intensity (A)	Energy consumption (kWh/m^3)
0–10	8.84	7.07	8.65	4.61	8.68	3.09
0–25	8.89	7.11	8.70	4.64	8.78	3.12
0–45	8.84	7.07	8.70	4.64	8.73	3.10
0–60	8.84	7.07	8.70	4.74	8.73	3.10

Table 4
Energy consumption per chemical oxygen demand removed (kWh/kg COD) at voltage 8 V with Al and Fe electrodes

HRT (h)	0.50		0.33		0.22	
Interval (min)	Al electrodes	Fe electrodes	Al electrodes	Fe electrodes	Al electrodes	Fe electrodes
0–10	1.38	1.77	1.00	1.54	0.81	1.19
0–25	1.29	1.53	0.93	1.12	0.62	0.81
0–45	1.23	1.36	0.89	0.99	0.60	0.72
0–60	1.19	1.34	0.88	0.98	0.58	0.67

3.2. Influence of hydraulic retention time on current efficiency

To present a general trend of the degree of conversion of the electrodes (anodes) into the coagulant electrogenerated due to the passing current in the continuous EC process, the current efficiency during each interval time is depicted as a box plot in Fig. 3 for the process with 8 V and HRT of 0.22, 0.33 and 0.5 h working both with Al and Fe electrodes. Current efficiency was calculated as the coefficient of the real mass of anodic consumption and the theoretical mass consumption according to Faraday's Law [Eq. (9)]. For continuous EC with 8 V (at interval 0 to 10, 25, 45 and 60 min), HRT of 0.22, 0.33 and 0.5 h using Al electrodes, the current efficiencies were 74.4% ± 3.6%, 86.6% ± 1.9% and 96.4% ± 4.1%, respectively. Regarding the Fe electrodes, at the same HRT, the values were 45.9% ± 0.3%, 56.4% ± 1.8% and 72.0% ± 3.3%, respectively. The electrocoagulation process with Al electrodes has always higher current efficiencies with respect to Fe electrodes. In addition, Table 5 shows in each time interval the consumption of electrodes per unit volume of wastewater treated for each HRT analyzed, the result is a double consumption rate for Fe electrodes with respect to Al electrodes. At HRT: 0.33 h (15 L/h) and 60 min operating time, for instance, the electrode consumption rates were 0.33 and 0.65 kg/m^3 of treated water for Al and Fe electrodes, respectively.

3.3. Influence of hydraulic retention time on current density

Fig. 4 shows the variations of the current densities and their tendency to stabilization working both with Al and Fe electrodes, clearly an indicative of non-passivation of the electrodes [53]. For the process with 8 V and HRT of 0.22, 0.33 and 0.5 h using Al electrodes, the current densities stabilized at values of 82.91, 82.05 and 81.20 A/m^2. In each case, the average values at 60 min were 81.54 ± 3.39, 78.89 ± 4.80 and 78.85 ± 3.67 A/m^2, respectively. Regarding the Fe electrodes, the values stabilized at the same time were 80.34, 78.63 and 79.49 A/m^2 and their average values of 78.60 ± 3.93, 76.75 ± 3.35 and 77.52 ± 3.97 A/m^2, respectively. The electrocoagulation process with Al electrodes has higher current densities with respect to Fe electrodes at 2.94, 2.14 and 1.33 A/m^2, respectively. For the three applied flow rates: 10, 15 and 22.5 L/h, the HRT were 0.50 h, 0.33 h and 0.22 h. In other research with slaughterhouse wastewater using Al electrodes with a flow rate of 1.62 L/h and HRT: 60 min the current density was 40 A/m^2 [52].

3.4. Influence of hydraulic retention time on pH

Fig. 5 shows how pH changes under the effects of the hydraulic retention time indicated above working with Al and Fe electrodes, as well as their stabilization trend. During the electrocoagulation process, the formation of the different Fe or Al species derived from these electrodes is influenced by the pH of the medium [54,55] and determines the performance of the process [56,57]. With the Al electrodes, the final pH values were 9.7, 8.65 and 8.38, and their average values were 8.65 ± 0.60, 8.34 ± 0.45 and 8.10 ± 0.45, respectively. In each case, pH increases were 1.57, 1.18 and 1.25. When the pH of the aqueous solution to be treated is in the range of 4–9, it will increase [58]. Regarding the Fe electrodes, the values at the end of the process were 9.54, 9.32

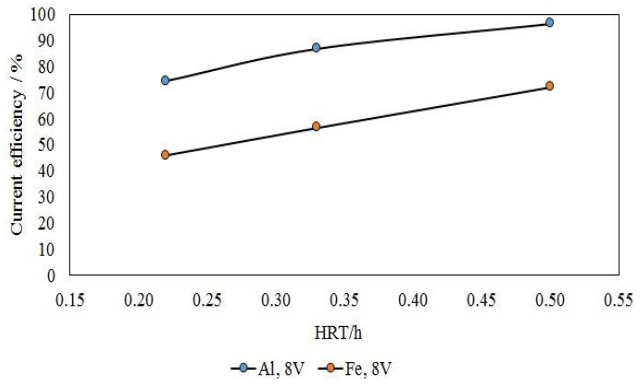

Fig. 3. Box plot for the influence of hydraulic retention time on the behavior of the current efficiency.

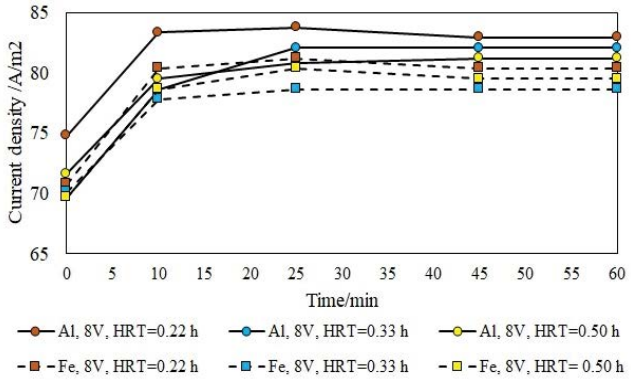

Fig. 4. Influence of hydraulic retention time on the behavior of the current density (A/m^2).

Table 5
Electrode consumption per m^3 of treated water (kg/m^3) at voltage 8 V with Al and Fe electrodes

HRT (h)	0.50		0.33		0.22	
Interval (min)	Al electrodes	Fe electrodes	Al electrodes	Fe electrodes	Al electrodes	Fe electrodes
0–10	0.57	1.43	0.34	0.70	0.18	0.37
0–25	0.60	1.31	0.35	0.70	0.21	0.38
0–45	0.60	1.29	0.35	0.67	0.20	0.37
0–60	0.61	1.28	0.33	0.65	0.19	0.37

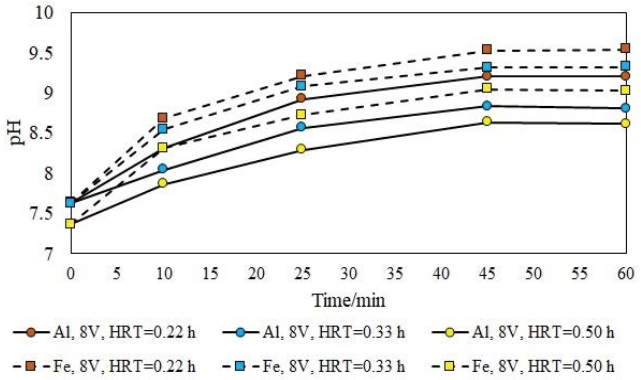

Fig. 5. Influence of hydraulic retention time on the behavior of pH.

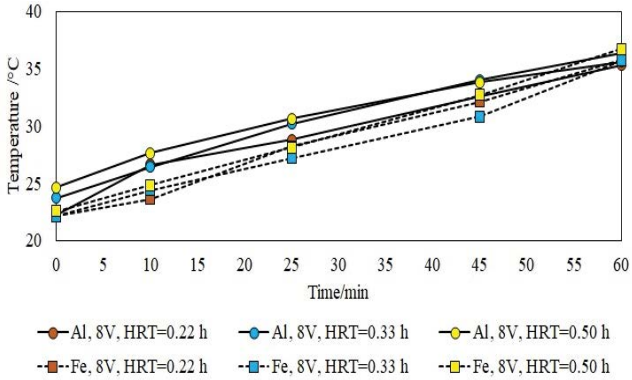

Fig. 6. Influence of hydraulic retention time on temperature behavior.

and 9.02 with average values of 8.92 ± 0.71, 8.77 ± 0.64 and 8.49 ± 0.62, respectively. In each case, the pH profiles for Fe electrodes are always above the pH profiles for Al electrodes. The migration of the OH^- ion from the cathode to the anode increases the pH of the anodic zone [59], favoring the formation of ferrous hydroxide [Eq. (2)] [60]. If the medium is acid, ferric hydroxide will be formed [Eq. (4)]. The cathodic reaction given by [Eq. (6)] shows the formation of hydroxyl ions, which increase the pH. The observed pH differences are a consequence of the different mechanisms with which the in situ generated coagulants act at pH > 7. The surfaces of these coagulants are positively charged and have the capacity to adsorb contaminants [58]. In addition, hydrogen and oxygen [Eq. (5)] gases adhere to the formed flocs, helping the electroflotation of the contaminants [61,62].

With the aluminum electrodes, the final pH values were 9.7, 8.65 and 8.38, and their average values were 8.65 ± 0.60, 8.34 ± 0.45 and 8.10 ± 0.45, respectively. The pH increases in each case were 1.57, 1.18 and 1.25. When the pH of the aqueous solution to be treated is in the range of 4–9, it will increase [58]. Regarding the iron electrodes, the values at the end of the process were 9.54, 9.32 and 9.02 with average values of 8.92 ± 0.71, 8.77 ± 0.64 and 8.49 ± 0.62, respectively. The pH profiles for iron electrodes in each case are always above the pH profiles for aluminum electrodes. The migration of the OH^- ion from the cathode to the anode increases the pH of the anodic zone [59], favoring the formation of ferrous hydroxide [Eq. (2)] [60]; if the medium is acid, ferric hydroxide will be formed [Eq. (4)].The cathodic reaction given by [Eq. (6)] shows the formation of hydroxyl ions, which increase the pH. The observed pH differences are a consequence of the different mechanisms with which the *in-situ* generated coagulants act at pH > 7. The surfaces of these coagulants are positively charged and have the capacity to adsorb contaminants [58]. In addition, hydrogen and oxygen [Eq. (5)] gases adhere to the formed flocs, helping the electroflotation of the contaminants [61,62].

3.5. Influence of hydraulic retention time on temperature

Fig. 6 shows the behavior of the temperature with the voltage and different HRT of the wastewater to be treated. The temperature profiles with both Fe and Al electrodes show a linear behavior. In all the cases, for the same HRT, the temperature profile using Al electrodes is slightly higher than the temperature profile using Fe electrodes. At the end of the process the temperature fluctuated between 35°C–37°C. The conversion of electrical energy into thermal energy increases the temperature, and is due to the electrical resistance of the aqueous medium. This physical phenomenon is known as the Joule effect [63–65].

Al, 10 L/h HRT = 0.22 h	$T = 0.2086t + 23.415$ $dT/dt = 0.2086$°C/min 81.54 ± 3.39 A/m²	$R^2 = 0.9729$
Al, 15 L/h HRT = 0.33 h	$T = 0.1792t + 25.427$ $dT/dt = 0.1792$°C/min 78.89 ± 4.80 A/m²	$R^2 = 0.9788$
Al, 22.5 L/h HRT = 0.50 h	$T = 0.1792t + 25.427$ $dT/dt = 0.1792$°C/min 78.85 ± 3.67 A/m²	$R^2 = 0.9788$
Fe, 10 L/h	$T = 0.2314t + 21.887$ $dT/dt = 0.2314$°C/min 78.60 ± 3.93 A/m²	$R^2 = 0.9943$
Fe, 15 L/h	$T = 0.2163t + 21.99$ $dT/dt = 0.2236$°C/min 76.75 ± 3.35 A/m²	$R^2 = 0.9869$
Fe, 22.5 L/h	$T = 0.2341t + 22.412$ $dT/dt = 0.2341$°C/min 77.52 ± 3.97 A/m²	$R^2 = 0.9988$

3.6. Influence of hydraulic retention time on turbidity

Fig. 7 shows the removal of turbidity with Al and Fe electrodes. When the flow of wastewater to be treated increases, the yields decrease with both electrodes. The best performances are achieved with Al electrodes. For these electrodes there are no differences when the wastewater flows were 10 and 15 L/h with average current densities of 81.54 ± 3.39 A/m² and 78.89 ± 4.80 A/m² in a time of 60 min. The yields achieved were of 99.46% and 99.47%, respectively. When the flow was 22.5 L/h with an average current density of 78.85 ± 3.67 A/m² at 60 min of EC process, the

yield was 98.71%. With the Fe electrode at 60 min of process with flows and average current densities of (10 L/h, 78.60 ± 3.93 A/m^2), (15 L/h, 76.75 ± 3.35 A/m^2) and (22.5 L/h, 77.52 ± 3.97 A/m^2), the yields were 96.44%, 94.49% and 93.39%, respectively. When HRT increases also performance increases. The same effect was found by [53,66].

3.7. Influence of hydraulic retention time on chemical oxygen demand

Fig. 8 shows the percentage of COD removal. Working with Al electrodes, higher yields were obtained with respect to Fe electrodes. After 60 min and HRT of 0.22, 0.33 and 0.50 h, the yields with the Al and Fe electrodes were 65.18%, 62.22% and 53.18% and 56.96%, 51.21% and 48.63%, respectively. Process efficiency decreased with increasing wastewater inflow rate or decreasing HRT. Other research also show the same trend [66,67].

3.8. Isothermal models of electrocoagulation–flotation kinetics

Tables 6 and 7 show the kinetic parameters q_e and k_n for both, working with Al and Fe electrodes, considering constant temperature during the EC process, q_e and k_1 for pseudo-first-order [Eq. (16)], and q_e and k_2 for pseudo-second-order [Eq. (18)] calculated by plotting linearization where q_e comes from the slope and k_n comes from the intercept. While those kinetic constants q_e and k_n were obtained by a non-linearized method by adjusting experimental values

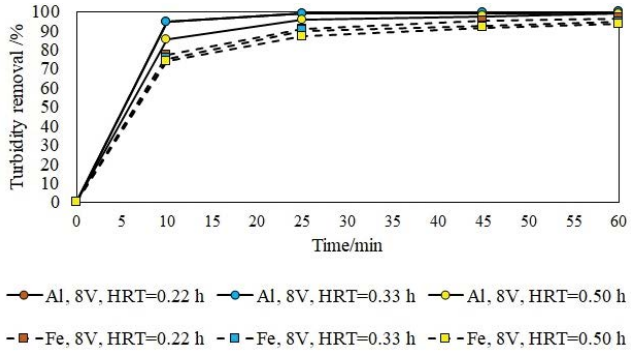

Fig. 7. Influence of hydraulic retention time on the percentage of turbidity removal.

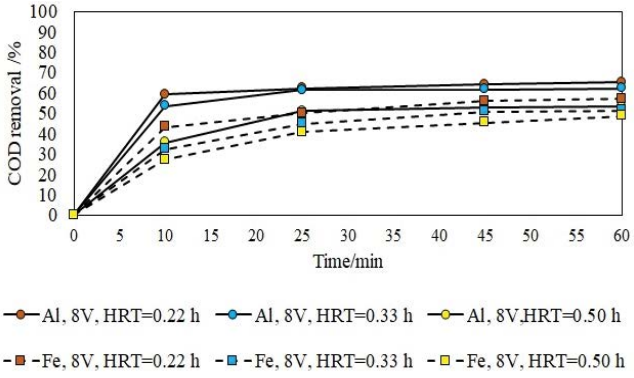

Fig. 8. Influence of hydraulic retention time on the percentage of chemical oxygen demand removal.

Table 6
Summary of the kinetic parameters and the isothermal model fitting for continuous EC at 8 V with Al electrodes at different hydraulic retention times

HRT (h)	0.50			0.33			0.22		
Electrode consumption W (g/h)	6.10			5.06			4.36		
Model	q_e	k_n	R^2	q_e	k_n	R^2	q_e	k_n	R^2
Linear pseudo-first-order (n = 1)	9,886.3	1.89E-1	0.993	16,206.3	1.05E-1	0.946	28,245.2	8.69E-2	0.971
Linear pseudo-second-order (n = 2)	9,973.6	1.66E-4	0.996	16,749.8	1.95E-5	0.995	30,026.5	6.51E-6	0.996
Non-linear pseudo-first-order (ExpDecay)	9,784.6	1.41E-1	0.968	15,892.4	1.32E-1	0.979	27,677.7	1.12E-1	0.996
Non-linear pseudo-second-order (FracDecay)	9,962.5	8.89E-5	1.000	16,541.0	2.95E-5	1.000	30,717.4	6.29E-6	0.997

Table 7
Summary of the kinetic parameters and the isothermal model fitting for continuous EC at 8 V with Fe electrodes at different hydraulic retention times

HRT (h)	0.50			0.33			0.22		
Electrode consumption W (g/h)	12.69			9.76			8.32		
Model	q_e	k_n	R^2	q_e	k_n	R^2	q_e	k_n	R^2
Linear pseudo-first-order (n = 1)	4,158.2	8.46E-2	0.950	7,398.0	6.98E-2	0.977	12,704.8	6.57E-2	0.991
Linear pseudo-second-order (n = 2)	4,614.6	3.14E-5	0.984	8,568.8	1.12E-5	0.991	14,663.6	6.25E-6	0.999
Non-linear pseudo-first-order (ExpDecay)	4,122.6	9.82E-2	0.975	7,286.4	9.12E-2	0.998	12,583.0	6.76E-2	0.993
Non-linear pseudo-second-order (FracDecay)	4,394.3	5.62E-5	0.998	8,446.3	1.42E-5	0.999	14,781.0	6.13E-6	0.999

to the respective equations for COD decay concentrations, that is, for pseudo-first-order, n = 1 [Eq. (30)] and for pseudo-second-order, n = 2 [Eq. (33)]. The mentioned tables also present the coefficients of determination R^2 of the isothermal models, which represents the conformity between the model values and experimental data [68], for the continuous EC process at 8 V and for each analyzed HRT. The comparison of the kinetic models shows that the kinetics of the reaction follows the pseudo-second-order model, since the R^2 for the pseudo first order kinetic models are relatively smaller than the R^2 of the pseudo-second-order kinetic models for the adsorption of COD using Al electrodes as well as Fe electrodes. Fig. 9 (linear pseudo-first-order) and Fig. 10 (linear pseudo-second-order), as well as, Fig. 11 (non-linear pseudo-first-order) and Fig. 12 (non-linear pseudo-second-order) show the experimental and predicted values for COD removal by continuous EC process at 8 V and for three HRT: 0.22, 0.33 and 0.5 h. Predicted values were previously calculated by considering a plotting linearization (Figs. 9 and 10) and by adjusting to an equation of kinetics decay (Figs. 11 and 12), respectively. For both cases, pseudo-first-order models (Figs. 9 and 11) have a notorious deviation for predicted values before 25 min, and are not suitable to predict COD removal further from equilibrium. Based on determination coefficients for comparing pseudo-second-order models, that is, linear pseudo-second-order and non-linear pseudo-second-order (FracDecay) with Al electrodes shown in Table 6, R^2 were (0.995–0.996 and 0.997–1.000), and with Fe electrodes shown in Table 7, R^2 were (0.984–0.999 and 0.998–0.999), respectively. It was found that the experimental data fitted better with pseudo-second-order isothermal model assessing R^2 = 0.997–1.000 for continuous EC process working both with Al and Fe electrodes. The operating parameters considered for non-linear pseudo-second-order (FracDecay) kinetic model were: volumetric flow rate (HRT, L/h), initial COD concentration (mg/L) and electrode consumption rate (g/h) for EC process at constant voltage of 8 V, and, considering an adsorption rate (k_n) at constant temperature. Moreover, the effects of the initial concentration on the removal efficiency of organic contaminants were analyzed in continuous EC for wastewater from the livestock industry of slaughterhouses by [52].

Similarly, previous studies on the kinetic removal of organic contaminants by EC process using Al electrodes [68,69] showed an excellent fit of the pseudo-second-order model and also the chemisorption of amorphous $Al(OH)_3(s)$,

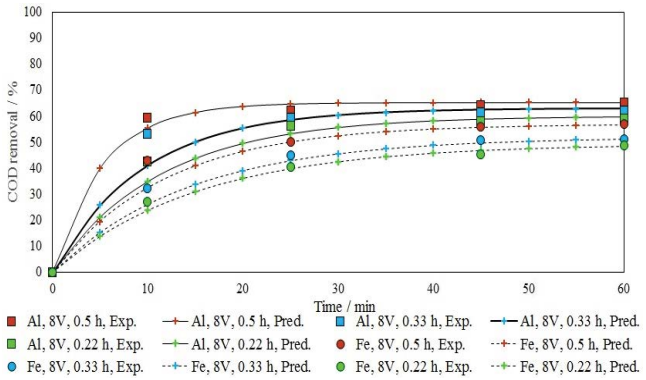

Fig. 9. COD removal efficiency using continuous EC at 8 V and different volumetric flow rates. Experimental and predicted values considering isothermal pseudo-first-order linear model.

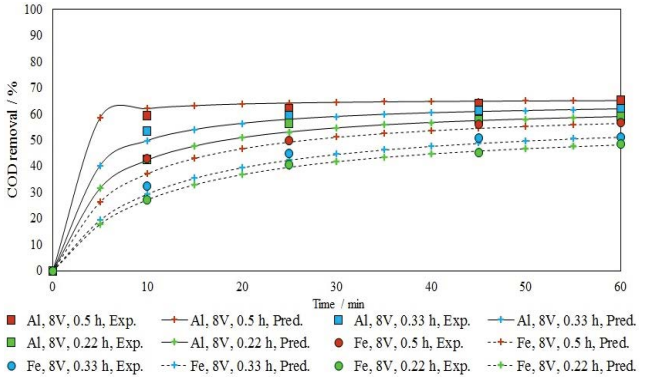

Fig. 10. COD removal efficiency using continuous EC at 8 V and different volumetric flow rates. Experimental and predicted values considering isothermal pseudo-second-order linear model.

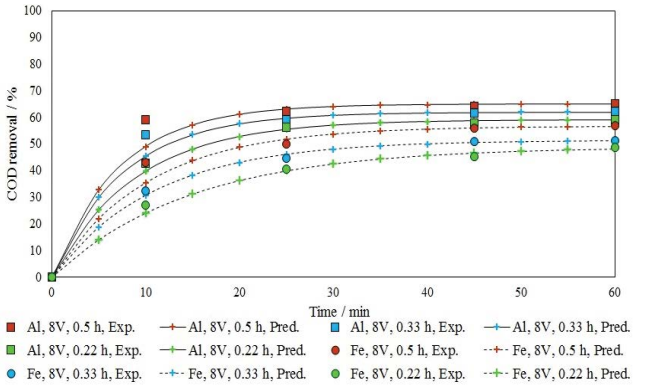

Fig. 11. COD removal efficiency using continuous EC at 8 V and different volumetric flow rates. Experimental and predicted values considering isothermal exponential decay model (ExpDecay).

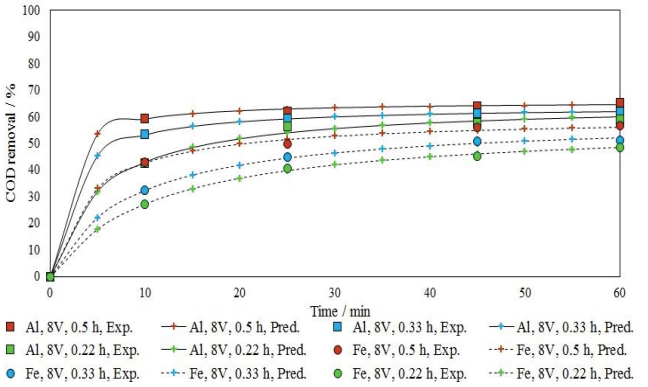

Fig. 12. COD removal efficiency using continuous EC at 8 V and different volumetric flow rates. Experimental and predicted values considering isothermal fractional decay model (FracDecay).

monomeric aluminum cations $Al(OH)^{2+}$(aq), $Al(OH)_2^+$(aq), and polymeric hydroxy chains, such as $Al_2(OH)_2^{4+}$(aq) and $Al_6(OH)_{15}^{3+}$(aq), which involves electron transfer between that species and pollutants as the dominant pathway during EC process. The polymeric chains are large surface area species and cause adsorption of entrapment of soluble organic and inorganic compounds as well as colloidal particles. The adsorption and entrapment will separate from the solution by settlement or floating by bubbles [70]. The inverse relationship between the hydraulic retention time and the equilibrium adsorption capacity (q_e) is noteworthy, which is attributed to a lower consumption of electrodes and a higher COD is eliminated as the HRT values decrease, which is indicative. of a good loading capacity on the surface of the coagulant generated. In addition, in all cases the results show that the adsorption capacities are always higher for Al electrodes with respect to Fe electrodes, this is related to the large surface area of aluminum polymeric species.

3.9. Method for non-isothermal kinetic adsorption

Tables 8 and 9 show the kinetic parameters q_e, k_0 and E_a for both, working with Al and Fe electrodes, considering temperature linear variation during the EC process due to Joule's effect. The kinetic parameters were calculated by plotting linearization and iteration for pseudo-first-order [Eq. (24)], and for pseudo-second-order [Eq. (25)] assuming a constant temperature slope (β). The mentioned tables present the determination coefficients (R^2) of the non-isothermal models for the EC process at 8 V and for each analyzed HRT. Similar to isothermal models, the reaction kinetic is more likely to follow the pseudo-second-order, since R^2 for pseudo-first-order kinetic models were relatively lower than those for pseudo-second-order kinetic models for COD adsorption using Al electrodes as well as with Fe electrodes. Fig. 13 (linear non-isothermal pseudo-first-order) and Fig. 14 (linear non-isothermal pseudo-second-order) show the experimental and predicted values for COD removal by continuous EC process at 8 V and for three HRT: 0.22, 0.33 and 0.5 h. The determination coefficients for linear non-isothermal pseudo-first-order and linear non-isothermal pseudo-second-order with Al electrodes shown in Table 8, R^2 were (0.431–0.787 and 0.860–0.999), and with Fe electrodes shown in Table 9, R^2 were (0.866–0.963 and 0.960–0.995), respectively.

It has been observed that the experimental data best fit the non-isothermal pseudo-second-order model for the continuous EC process with Al and Fe electrodes, and several values were obtained that do not fit properly when $R^2 < 0.95$. The activation energies of the kinetic reaction were

Table 8
Summary of the kinetic parameters and the non-isothermal model fitting for continuous EC at 8 V with Al electrodes at different hydraulic retention times

HRT (h)	0.50		0.33		0.22	
Electrode consumption W (g/h)	6.10		5.06		4.36	
Parameter	Linear pseudo-first-order non-isothermal	Linear pseudo-second-order non-isothermal	Linear pseudo-first-order non-isothermal	Linear pseudo-second-order non-isothermal	Linear pseudo-first-order non-isothermal	Linear pseudo-second-order non-isothermal
q_e	9,886.3	9,973.6	16,206.3	16,749.8	28,245.2	30,026.5
k_0	7.37E+15	1.24E+13	3.40E+13	2.32E+15	1.28E+22	2.17E+17
E_a	96,650	97,807	85,195	116,999	135,688	131,222
R^2	0.787	0.999	0.570	0.876	0.431	0.860

Table 9
Summary the kinetic parameters and the non-isothermal model fitting for continuous EC at 8 V with Fe electrodes at different hydraulic retention times

HRT (h)	0.50		0.33		0.22	
Electrode consumption W (g/h)	12.69		9.76		8.32	
Parameter	Linear pseudo-first-order non-isothermal	Linear pseudo-second-order non-isothermal	Linear pseudo-first-order non-isothermal	Linear pseudo-second-order non-isothermal	Linear pseudo-first-order non-isothermal	Linear pseudo-second-order non-isothermal
q_e	4,158.2	4,614.6	7,398.0	8,568.8	12,704.8	14,663.6
k_0	2.61E+4	6.99E-1	1.58E+0	1.97E-2	1.48E+4	1.39E-2
E_a	32,276	25,642	8,956	19,358	31,502	19,926
R^2	0.866	0.960	0.963	0.974	0.947	0.995

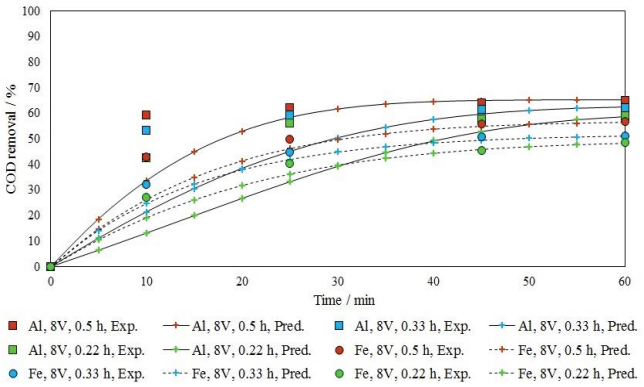

Fig. 13. COD removal efficiency using continuous EC at 8 V and different volumetric flow rates. Experimental and predicted values considering the non-isothermal pseudo-first-order model.

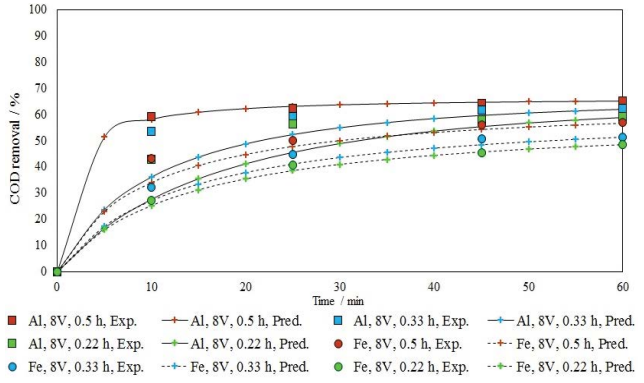

Fig. 14. COD removal efficiency using continuous EC at 8 V and different volumetric flow rates. Experimental and predicted values considering the non-isothermal pseudo-second-order model.

calculated from the slope of the linearized equation [Eq.(26)] for Al electrodes were 97.8–131.2 kJ/mol higher than the values for Fe electrodes 8.9–25.6 kJ/mol indicating domination of activated chemisorption phenomena for EC process. The operating parameters considered for the non-linear pseudo-second-order (FracDecay) kinetic model were: hydraulic retention time (HRT, h); initial COD concentration (mg/L); and electrode consumption rate (g/h) for EC process at constant voltage of 8 V; and considering an adsorption rate (k_n) at constant temperature. For the non-linear pseudo-second-order model (FracDecay), temperature is not a significant parameter to model COD removal for continuous EC due to the decrease in R^2.

4. Conclusions

Electrocoagulation is an electrochemical technology and was applied to investigate the influence of hydraulic retention time on the removal of COD in continuous mode as primary treatment for wastewater from slaughterhouses. This technology applied as a continuous mode process is strongly dependent on the hydraulic retention time, and its application is viable for this type of wastewater. The experimental data were analyzed using pseudo-first-order and pseudo-second-order kinetic equations considering isothermal and non-isothermal conditions, and it was found that the data best fit the pseudo-second-order isothermal model with R^2 = 0.997–1.000, in both cases working with electrodes of Al and Fe.

Conflicts of interest

The authors declare no conflict of interest, financial, or otherwise.

Acknowledgment

The authors wish to thank Esmeralda Corp. S.A.C. for their financial support and for allowing us to use their facilities for research work.

References

[1] C. Bustillo-Lecompte, M. Mehrvar, E. Quiñones-Bolaños, Slaughterhouse wastewater characterization and treatment: an economic and public health necessity of the meat processing industry in Ontario, Canada, J. Geosci. Environ. Prot., 4 (2016) 175–186, doi: 10.4236/gep.2016.44021.
[2] C.J. Banks, Z. Wang, Treatment of Meat Wastes, In: Waste Treatment in the Food Processing Industry, 1st ed., CRC Press, United States, 2004, pp. 67–100.
[3] A. Gutiérrez-Sarabia, G. Fernandez-Villagómez, P. Martínez-Pereda, N. Rinderknecht-Seijas, H.M. Poggi-Varaldo, Slaughterhouse wastewater treatment in a full-scale system with constructed wetlands, Water Environ. Res., 76 (2004) 334–343.
[4] J.T. Nwabanne, C.C. Obi, Abattoir wastewater treatment by electrocoagulation using iron electrodes, Pelagia Res. Lib., 8 (2017) 254–260.
[5] I. Hamawand, Anaerobic digestion process and bio-energy in meat industry: a review and a potential, Renewable Sustainable Energy Rev., 44 (2015) 37–51.
[6] J. Li, M.G. Healy, X. Zhan, D. Norton, M. Rodgers, Effect of aeration rate on nutrient removal from slaughterhouse wastewater in intermittently aerated sequencing batch reactors, Water Air Soil Pollut., 192 (2008) 251–261.
[7] C. Bustillo-Lecompte, M. Mehrvar, Slaughterhouse Wastewater: Treatment, Management and Resource Recovery, R. Farooq, Z. Ahmad, Eds., Physico-Chemical Wastewater Treatment and Resource Recovery, InTechOpen, United Kingdom, 2017, pp. 153–174.
[8] G.Th. Kroyer, Impact of food processing on the environment—an overview, LWT Food Sci. Technol., 28 (1995) 547–552.
[9] V. Yargeau, Water and Wastewater Treatment: Chemical Processes, Metropolitan Sustainability: Understanding and Improving the Urban Environment, Woodhead Publishing Limited, Canada, 2012, pp. 390–405.
[10] R.D. Lettermann, A. Amirtharajah, C.R. O'Melia, Coagulation and Floculation, In: Water Quality and Treatment, 5th ed., United States, 2000, pp. 297–362.
[11] M.V.B. Gonçalves, S.C. De Oliveira, B.M.P.N. Abreu, E.M. Guerra, D.T. Cestarolli, Electrocoagulation/electroflotation process applied to decolourization of a solution containing the Dye Yellow Sirius K-CF, Int. J. Electrochem. Sci., 11 (2016) 7576–7583.
[12] B.S. Yildiz, Water and Wastewater Treatment: Biological Processes, In: Metropolitan Sustainability Understanding and Improving the Urban Environment, Woodhead Publishing Limited, United Kingdom, 2012, pp. 406–428.
[13] N. Oturan, M.A. Oturan, Chapter 8 – Electro-Fenton Process: Background, New Developments, and Applications, C.A. Martínez-Huitle, M.A. Rodrigo, O. Scialdone, Eds., Electrochemical Water and Wastewater Treatment, Butterworth-Heinemann, United Kingdom, 2018, pp. 193–221.

[14] D. Al deen Atallah Aljuboury, P. Palaniandy, H.A. Aziz, S. Feroz, A review on the fenton process for wastewater treatment, J. Innovative Eng., 2 (2014) 1–22.
[15] C.E. Barrera-Díaz, P. Balderas-Hernández, B. Bilyeu, Chapter 3 – Electrocoagulation: Fundamentals and Prospectives, C.A. Martínez-Huitle, M.A. Rodrigo, O. Scialdone, Eds., Electrochemical Water and Wastewater Treatment, Butterworth-Heinemann, United Kingdom, 2008, pp. 61–76.
[16] S.H. Abbas, W.H. Ali, Electrocoagulation technique used to treat wastewater: a review, Am. J. Eng. Res., 7 (2018) 74–88.
[17] S. Thakur, M.S. Chauhan, Treatment of wastewater by electrocoagulation: a review, Int. J. Eng. Sci. Innovative Technol., 5 (2016) 104–110.
[18] M. Eyvaz, Treatment of brewery wastewater with electrocoagulation: improving the process performance by using alternating pulse current, Int. J. Electrochem. Sci., 11 (2016) 4988–5008.
[19] F. Ghanbari, M. Moradi, A. Eslami, M.M. Emamjomeh, Electrocoagulation/flotation of textile wastewater with simultaneous application of aluminum and iron as anode, Environ. Processes, 1 (2014) 447–457.
[20] A.I. Adeogun, R.B. Balakrishnan, Kinetics, isothermal and thermodynamics studies of electrocoagulation removal of basic dye rhodamine B from aqueous solution using steel electrodes, Appl. Water Sci., 7 (2017) 1711–1723.
[21] G. Chen, Electrochemical technologies in wastewater treatment, Sep. Purif. Technol., 38 (2004) 11–41.
[22] V. Kuokkanen, T. Kuokkanen, J. Rämö, U. Lassi, Recent applications of electrocoagulation in treatment of water and wastewater—a review, Green Sustainable Chem., 3 (2013) 89–121, doi: 10.4236/gsc.2013.32013.
[23] S. Ibrahim, N.S.M. Aris, B. Ariffin, Y. Hawari, M.A.K.M. Hanafiah, Application of electrocoagulation process for decolourisation of palm oil mill effluent (POME), Nat. Environ. Pollut. Technol.: An Int. Q. Sci. J., 17 (2018) 1267–1271.
[24] B.M.B. Ensano, L. Borea, V. Naddeo, V. Belgiorno, M.D.G. De Luna, F.C. Ballesteros, Removal of pharmaceuticals from wastewater by intermittent electrocoagulation, Water, 9 (2017) 85, doi: 10.3390/w9020085.
[25] E. Bazrafshan, F.K. Mostafapour, M. Farzadkia, K.A. Ownagh, A.H. Mahvi, Slaughterhouse wastewater treatment by combined chemical coagulation and electrocoagulation process, PLoS One, 7 (2012) e40108, doi: 10.1371/journal.pone.0040108.
[26] H. Liu, X. Zhao, J. Qu, Electrocoagulation in Water Treatment, In: Electrochemistry for the Environment, Springer, USA, 2010, pp. 245–262.
[27] I. Linares-Hernández, C. Barrera-Díaz, G. Roa-Morales, B. Bilyeu, F. Ureña-Núñez, Influence of the anodic material on electrocoagulation performance, Chem. Eng. J., 148 (2009) 97–105.
[28] A.A. Al-Raad, M.M. Hanafiah, A.S. Naje, M.A. Ajeel, A.O. Basheer, T.A. Aljayashi, M.E. Toriman, Treatment of saline water using electrocoagulation with combined electrical connection of electrodes, Processes, 7 (2019) 242, doi: 10.3390/pr7050242.
[29] W. Reátegui-Romero, L.V. Flores-Del Pino, J.L. Guerrero-Guevara, J. Castro-Torres, L.M. Rea-Marcos, M.E. King-Santos, R. Yuli-Posadas, Benefits of electrocoagulation in treatment of wastewater: removal of Fe and Mn metals, oil and grease and COD: three case studies, Int. J. Appl. Eng. Res., 13 (2018) 6450–6462.
[30] M. Kobya, O.T. Can, M. Bayramoglu, Treatment of textile wastewaters by electrocoagulation using iron and aluminum electrodes, J. Hazard. Mater., 100 (2003) 163–178.
[31] O.T. Can, M. Kobya, E. Demirbas, M. Bayramoglu, Treatment of the textile wastewater by combined electrocoagulation, Chemosphere, 62 (2006) 181–187.
[32] H. Tounsi, T. Chaabane, K. Omine, V. Sivasankar, H. Sano, M. Hecini, A. Darchen, Electrocoagulation in the dual application on the simultaneous removal of fluoride and nitrate anions through respective adsorption/reduction processes and modelling of continuous process, J. Water Process Eng., 46 (2022) 102584, doi: 10.1016/j.jwpe.2022.102584.
[33] W. Reátegui-Romero, S.A. Tuesta-Tinoco, C.E. Ochoa De la Cruz, J.A. Huamán-Ccopa, M.E. King-Santos, E.F. Estrada-Huamaní, W. Bulege-Gutierrez, R.A. Yuli-Posadas, V. Fernández-Guzmán, Electrocoagulation in batch mode for the removal of the chemical oxygen demand of an effluent from slaughterhouse wastewater in Lima Peru: Fe and Al electrodes, Desal. Water Treat., 202 (2020) 206–218.
[34] A.I. Adeogun, R.B. Balakrishnan, Kinetics, isothermal and thermodynamics studies of electrocoagulation removal of basic dye rhodamine B from aqueous solution using steel electrodes, Appl. Water Sci., 7 (2015) 1711–1723.
[35] E. Ajenifuja, J.A. Ajao, E.O.B. Ajayi, Adsorption isotherm studies of Cu(II) and Co(II) in high concentration aqueous solutions on photocatalytically modified diatomaceous ceramic adsorbents, Appl. Water Sci., 7 (2017) 3793–3801.
[36] T.R. Sahoo, B. Prelot, Chapter 7 – Adsorption Processes for the Removal of Contaminants From Wastewater: The Perspective Role of Nanomaterials and Nanotechnology, B. Bonelli, F.S. Freyria, I. Rossetti, R. Sethi, Eds., Nanomaterials for the Detection and Removal of Wastewater Pollutants: Micro and Nano Technologies, Elsevier, United States, 2020, pp. 161–222.
[37] A.S. Yusuff, L.T. Popoola, E.O. Babatunde, Adsorption of cadmium ion from aqueous solutions by copper-based metal organic framework: equilibrium modeling and kinetic studies, Appl. Water Sci., 9 (2019) 106, doi: 10.1007/s13201-019-0991-z.
[38] C.N. Owabor, I.O. Oboh, Kinetic study and artificial neural network modeling of the adsorption of naphthalene on grafted clay, J. Eng. Res., 16 (2012) 41–51.
[39] B. Nagy, C. Mânzatu, A. Măicăneanu, C. Indolean, B.-T. Lucian, C. Majdik, Linear and non-linear regression analysis for heavy metals removal using *Agaricus bisporus* macrofungus, Arabian J. Chem., 10 (2017) S3569–S3579.
[40] E.D. Revellame, D.L. Fortela, W. Sharp, R. Hernandez, M.E. Zappi, Adsorption kinetic modeling using pseudo-first order and pseudo-second-order rate laws: a review, Cleaner Eng. Technol., 1 (2020) 100032, doi: 10.1016/j.clet.2020.100032.
[41] K.D. Kowanga, E. Gatebe, G.O. Mauti, E.M. Mauti, Kinetic, sorption isotherms, pseudo-first-order model and pseudo-second-order model studies of Cu(II) and Pb(II) using defatted *Moringa oleifera* seed powder, J. Phytopharmacol., 5 (2016) 71–78.
[42] H. Yuh-Shan, Citation review of Lagergren kinetic rate equation on adsorption reactions, Scientometrics, 59 (2004) 171–177.
[43] Y.S. Ho, J.C.Y. Ng, G. McKay, Kinetics of pollutant sorption by biosorbents: review, Sep. Purif. Methods, 29 (2000) 189–232.
[44] S. Lagergren, Zur theorie der sogenannten adsorption geloster stoffe, Kungliga Svenska Vetenskapsakademiens, 24 (1898) 1–39.
[45] A. Othmani, A. Kesraoui, M. Seffen, The alternating and direct current effect on the elimination of cationic and anionic dye from aqueous solutions by electrocoagulation and coagulation flocculation, Euro-Mediterr. J. Environ. Integr., 2 (2017) 1–12, doi: 10.1007/s41207-017-0016-y.
[46] S. Lyubchik, E. Lygina, A.I. Lyubchyk, S.B. Lyubchik, J.M. Loureiro, I.M. Fonseca, A.B. Ribeiro, M.M. Pinto, A.M. Sá Figueiredo, The Kinetic Parameters Evaluation for the Adsorption Processes at "Liquid–Solid" Interface, A.B. Ribeiro, E.P. Mateus, N. Couto, Eds., Electrokinetics Across Disciplines and Continents. New Strategies for Sustainable Development, Springer International Publishing, Switzerland, 2016, pp. 81–109.
[47] Y.-S. Ho, Review of second-order models for adsorption systems, J. Hazard. Mater., 136 (2006) 681–689.
[48] Y.S. Ho, G. McKay, Pseudo-second-order model for sorption processes, Process Biochem., 34 (1999) 451–465.
[49] P. Ganesan, J. Lakshmi, G. Sozhan, S. Vasudevan, Removal of manganese from water by electrocoagulation: adsorption, kinetics and thermodynamic studies, Can. J. Chem. Eng., 91 (2013) 1–11, doi: 10.1002/cjce.21709.
[50] X.-Y. Yang, B. Al-Duri, Application of branched pore diffusion model in the adsorption of reactive dyes on activated carbon, Chem. Eng. J., 83 (2001) 15–23.
[51] R.E. Lyon, An integral method of non-isothermal kinetic analysis, Thermochim. Acta, 297 (1997) 117–124.

[52] M.S. Hellal, H.S. Doma, E.M. Abou-Taleb, Techno-economic evaluation of electrocoagulation for cattle slaughterhouse wastewater treatment using aluminum electrodes in batch and continuous experiment, Sustainable Environ. Res., 33 (2023) 1–12, doi: 10.1186/s42834-023-00163-0.
[53] T.L. Benazzi, M. Di Luccio, R.M. Dallago, J. Steffens, R. Mores, M.S. Do Nascimento, J. Krebs, G. Ceni, Continuous flow electrocoagulation in the treatment of wastewater from dairy industries, Water Sci. Technol., 73 (2016) 1418–1425.
[54] S.R. Tchamango, K.W. Ngayo, P.D.B. Belibi, F. Nkouam, M.B. Ngassoum, Treatment of a dairy effluent by classical electrocoagulation and indirect electrocoagulation with aluminum electrodes, Sep. Sci. Technol., 56 (2021) 1128–1139.
[55] M. Kobya, O.T. Can, M. Bayramoglu, Treatment of textile wastewaters by electrocoagulation using iron and aluminum electrodes, J. Hazard. Mater., 100 (2003) 163–178.
[56] G. Mouedhen, M. Feki, M. De Petris Wery, H.F. Ayedi, Behavior of aluminum electrodes in electrocoagulation process, J. Hazard. Mater., 150 (2008) 124–135.
[57] X. Chen, G. Chen, P.L. Yue, Separation of pollutants from restaurant wastewater by electrocoagulation, Sep. Purif. Technol., 19 (2000) 65–76.
[58] H. Liu, X. Zhao, J. Qu, Electrocoagulation in Water Treatment, in Electrochemistry for the Environment, Springer, USA, 2010, pp. 245–262.
[59] A.K. Prajapati, P.K. Chaudhari, Physicochemical treatment of distillery wastewater—a review, Chem. Eng. Commun., 202 (2015) 1098–1117.
[60] S.U. Khan, M. Khalid, K. Hashim, M.H. Jamadi, M. Mousazadeh, F. Basheer, I.H. Farooqi, Efficacy of electrocoagulation treatment for the abatement of heavy metals: an overview of critical processing factors, kinetic models and cost analysis, Sustainability, 15 (2023) 1708, doi: 10.3390/su15021708.
[61] R. Soni, S. Bhardwaj, D.P. Shukla, Chapter 14 – Various Water-Treatment Technologies for Inorganic Contaminants: Current Status and Future Aspects, P. Devi, P. Singh, S.K. Kansal, Eds., Inorganic Pollutants in Water, Elsevier, United States, 2020, pp. 273–295.
[62] H. Hu, K. Xu, Chapter 8 – Physicochemical Technologies for HRPs and Risk Control, H. Ren, X. Zhang, Eds., High-Risk Pollutants in Wastewater, Nanjing, China, Elsevier, United States, 2020, pp. 169–207.
[63] L.Shi, Z. Han, Y. Feng, C. Zhang, Q. Zhang, H. Zhu, S. Zhu, Joule heating of ionic conductors using zero-phase frequency alternating current to suppress electrochemical reactions, Engineering, 25 (2023) 138–143.
[64] D. Ghernaout, A.S. Alghamdi, B. Ghernaout, Electrocoagulation process: a mechanistic review at the dawn of its modeling, J. Environ. Sci. Allied Res., 2 (2019) 22–38.
[65] L.P. Cappato, M.V.S. Ferreira, J.T. Guimaraes, J.B. Portela, A.L.R. Costa, M.Q. Freitas, R.L. Cunha, C.A.F. Oliveira, G.D. Mercali, L.D.F. Marzack, A.G. Cruz, Ohmic heating in dairy processing: Relevant aspects for safety and quality, Trends Food Sci. Technol., 62 (2017) 104–112.
[66] M.A. Musa, S. Idrus, Effect of hydraulic retention time on the treatment of real cattle slaughterhouse wastewater and biogas production from HUASB reactor, Water, 12 (2020) 490, doi: 10.3390/w12020490.
[67] Y.D. Sağsöz, A.E. Yilmaz, F.E. Torun, B. Kocadağistan, S. Kul, The investigation of COD treatment and energy consumption of urban wastewater by a continuous electrocoagulation system, J. Electrochem. Sci. Technol., 13 (2022) 261–268.
[68] M. Wu, Y. Hu, R. Liu, S. Lin, W. Sun, H. Lu, Electrocoagulation method for treatment and reuse of sulphide mineral processing wastewater: characterization and kinetics, Sci. Total Environ., 696 (2019) 134063, doi: 10.1016/j.scitotenv.2019.134063.
[69] S. Kumari, R. Naresh Kumar, River water treatment by continuous electrocoagulation: insights into removal of acetaminophen, and natural organic matter, Water Supply, 22 (2022) 4055–4066.
[70] P. Kumar, T. Nawaz, S.P. Singh, Evaluation and optimization of electrocoagulation process parameters for the treatment of oil drill site wastewater, Chem. Eng. Ind. Chem., 1 (2022) 1–28.